# UAV-based Assessment of the Impact of Aboveground Biomass and Photosynthesis Parameters on Winter Wheat Yield

**JINGCHENG ZHANG[1], VLADYSLAV PITSYK[1] & KANG YU[1]**

*Abstract: The enhancement of grain yield (GY) in wheat (Triticum aestivum) is pivotal for global food security, yet it faces bottlenecks as potential yield improvements through traditional breeding reach their ceiling. This study investigated whether above-ground biomass (AGB) or photosynthetic efficiency parameters provide a more accurate mid-season prediction of GY in winter wheat.*

*Utilizing unmanned aerial vehicle (UAV) multispectral (MS) imagery, we extracted canopy reflectance data to evaluate the correlation of 35 vegetation indices (VIs) with AGB and key photosynthetic parameters across three phenological stages. Our analysis employed an array of computational techniques: principal component analysis (PCA), partial least squares regression (PLSR), random forest (RF), and support vector regression (SVR), each with distinctive approaches to model the relationship between VIs and GY.*

*The findings revealed that VIs have a pronounced correlation with AGB, particularly at the flowering stage, suggesting that AGB could serve as a more reliable predictor of GY than photosynthetic efficiency parameters. Among the modeling techniques, PLSR yielded the most accurate GY predictions across all stages. Notably, PCA and RF also demonstrated substantial predictive capabilities, with RF models providing robust performance and insightful variable importance metrics. SVR models, while exhibiting the need for careful normalization due to their sensitivity to data scaling, still performed commendably, especially in the grain ripening stage.*

*With the demonstrated promise of VIs as effective proxies for AGB, we recommend their integration into GY estimation models, contributing to developing a reliable indicator of yield forecasting and the optimization of resource allocation in agricultural practices.*

## 1 Introduction

The core of crop productivity lies photosynthesis, the process by which plants capture and store energy. Enhancements in photosynthetic efficiency, particularly the rate of $CO_2$ assimilation (A) per leaf area (FURBANK et al. 2020), can lead to yield increases (PARRY et al. 2010; RAINES 2010). This rate is a reflection of a plant's metabolic health (ZHANG et al. 2013), encapsulating the efficiency of carbon assimilation. It is a composite indicator, incorporating resource use efficiency (TARVAINEN et al. 2015), influenced by light (PENNISI et al. 2019), water (DONOHUE et al. 2017), and nutrient availability (TAUSZ-POSCH et al. 2014). Besides, stomatal conductance, denoted as 'gs', is also a vital physiological mechanism in plants that ensures gas exchange and significantly affects photosynthetic performance (TANAKA et al. 2013). It affects the diffusion of $CO_2$ into the leaf (YAMORI & SHIKANAI 2016), thereby impacting the rate of $CO_2$ assimilation (LAWSON et al. 2011). The significant natural variability of stomatal conductance observed in different plant species (FARALLI et al. 2019; ROCHE 2015), emphasizes its potential as a breeding target for increasing $CO_2$ assimilation and yield.

[1] Precision Agriculture Laboratory, School of Life Sciences, Technical University of Munich, D-85354 Freising, Germany, E-Mail: [Jingc.zhang, vladyslav.pitsyk, kang.yu]@tum.de

 DOI: 10.24407/KXP:1885707169

Chlorophyll fluorescence (ChlF) parameters, especially the maximum quantum efficiency of PSII (Fv/Fm and Fv'/Fm'), serve as reliable indicators of photosynthetic efficiency (GUIDI et al. 2019), plant health (BAURIEGEL et al. 2010), and stress detection (YAO et al. 2018). It has been emphasized as a useful tool for studying the photosynthetic mechanisms (GUIDI & CALATAYUD 2014; SÁNCHEZ-MOREIRAS et al. 2020).

While photosynthetic parameters offer a snapshot of plant physiology, above ground biomass (AGB) provides a cumulative measure of these processes over time. AGB represents the tangible outcome of photosynthetic activity, which is directly related to plant development and an essential determinant of yield (WALTER et al. 2018; YUE et al. 2019). Its variation among wheat cultivars highlights the influence of genetic and environmental factors on productivity (BENDIG et al. 2014). Thus, understanding the relationship between AGB and photosynthetic parameters is essential for predicting winter wheat yield, which is the focus of this study.

In the field of plant physiological research, conventional methodologies for quantifying photosynthetic efficiency and biomass accumulation are time-consuming and labour intensive. Advances in remote sensing technology, specifically unmanned aerial vehicle (UAV) systems equipped with multispectral (MS) and standard RGB cameras, have emerged as a non-invasive and expeditious alternative. These systems facilitate the remote assessment of critical agronomic traits, including grain yield (GY) (HERZIG et al. 2021), nitrogen (N) content (PREY & SCHMIDHALTER 2019), senescence patterns (MAKANZA et al. 2018), crop density (LIU et al. 2017), and plant height (LIU et al. 2021). The integration of UAV-derived datasets with advanced machine learning (ML) and deep learning (DL) algorithms offers a promising frontier for enhancing the precision of yield predictions (PAUDEL et al. 2022).

Notwithstanding the application of UASs and associated vegetation indices (VIs) in the analysis of GY, little is known about whether it is more important to monitor key photosynthetic parameters or AGB for predicting yield. This study postulated that AGB, due to its direct relation to biomass accumulation, will exhibit a more pronounced correlation with multispectral VIs, thereby serving as a superior predictive measure for GY.

The objectives of this investigation are i) to examine the correlations between photosynthetic parameters, AGB, and VIs with wheat GY; ii) to evaluate the performance of selected VIs and ML models in predicting wheat yield.

# 2 Materials and Methods

## 2.1 Study Area and Experimental Design

Seven diverse European winter wheat elite varieties were involved in this experiment, i.e., Aurelius (Saatbau Linz), Bernstein (Syngenta), Dagmar (Limagrain), Mv Nador (Marton genetics), Nogal (F. Desprez et Fils), Skyfall (R.A.G.T Saaten Deutschland), and Julius (KWS Lochow). These varieties were sown in plots that measured 10 m x 1.85 m, with a row spacing of 15 cm. The trial utilized a randomized complete block design, comprising four replicates and three nitrogen (N) treatments, resulting in a total of 84 plots. The experimental site was located at the research station of the Technical University of Munich in Dürnast, Freising (48.40630° N, 11.69535° E). The soil at this location is described as a homogeneous Cambisol with a composition of 20.8% clay, 61.5% silt, and 16.6% sand. Three N fertilizer levels (i.e., 0, 120, and 180 kg N $ha^{-1}$), which were chosen based on typical agronomic recommendations for winter wheat were implemented. These were applied in three equal portions around BBCH

25, 32, and 60 using Ammonium Sulphate Nitrate and Calcium Ammonium Nitrate. The soil was rich in P and K, so no additional application rate was added. Standard field management practices were uniformly applied across all plots. Sowing took place on 02.11.2022, and the crops were harvested upon reaching full maturity on 27.07.2023.

## 2.2 Data Collection and Methodology

### 2.2.1 Photosynthetic Parameter Quantification

This investigation delineated the photosynthetic dynamics of selected European winter wheat cultivars at critical phenological stages. The stages were characterized using the BBCH scale: BBCH40 (end of stem elongation), BBCH65 (flowering), and BBCH80 (grain filling and maturation). The LI-6800 Portable Photosynthesis System (LI-COR Biosciences, Lincoln, NE, USA) facilitated the quantification of key photosynthetic metrics: net assimilation rate (A), stomatal conductance to water vapor (gsw), and the efficiency of photosystem II photochemistry as indicated by chlorophyll fluorescence (Fv'/Fm'). The LI6800 provided data on four stomatal conductance parameters; however, this study focused on gsw due to its documented responsiveness to water related indices. Environmental conditions within the measurement chamber were rigorously regulated to ensure uniformity: airflow (700 µmol $s^{-1}$), relative humidity (55%), ambient $CO_2$ (400 ppm), chamber temperature (25°C), PAR (20 µmol $m^{-2}s^{-1}$), and light intensity for fluorescence measurements (200 µmol $m^{-2}s^{-1}$). Measurements were taken post-equilibration, averaging 40 to 60 seconds per sample. Three foliar samples per plot were analyzed, with mean values used for subsequent analysis.

### 2.2.2 Acquisition and Processing of Multispectral Images

Reflectance data was captured using a DJI Matrice M300 RTK UAV, equipped with a MicaSense Dual Camera Kit. This setup captured data across ten spectral bands, namely: blue (444 nm, 475 nm), green (531 nm, 560 nm), red (650 nm, 668 nm), red edge (705 nm, 717 nm, 740 nm), and near-infrared (840 nm). Radiometric correction was ensured by an onboard ambient light sensor and reflectance panels used for calibration. UAV flights were conducted at 12 meters AGL for optimal GSD (1.08 cm) with 80% overlap in all directions. Flight timing was synchronized with peak solar irradiance for consistency. Orthomosaics were generated in Agisoft Metashape Professional 1.8.4, with geospatial accuracy verified by the UAV's RTK-GPS and SAPOS. Spectral band calculations on orthomosaics were performed in QGIS 3.32.3, employing raster calculator tools and Excess Green Index-based segmentation to minimize soil background interference. The refined spectral indices were saved as TIFF files for correlation analyses within the R environment. In this study, a comprehensive suite of 35 VIs was meticulously chosen to forecast the yield of winter wheat cultivars. Specifically, 9 VIs were selected for their relationship to the assimilation rate and stomatal conductance, which are indicative of the plants' gaseous exchange capabilities. 16 VIs were included for their pertinence to chlorophyll fluorescence, serving as proxies for the efficiency of photosystem II photochemistry. The remaining 15 VIs were identified for their connection to AGB, reflecting the direct measure of crop development. The aggregation of these indices was aimed at harnessing their collective predictive power to enhance the accuracy of yield estimations, thereby addressing the critical intersection of photosynthetic activity and biomass accumulation. Computations were conducted in R, using the 'raster' package to manage zonal statistics and calculate median VI values for defined ROIs corresponding to experimental plots.

#### 2.2.3 Modelling Approaches and Evaluation

A suite of models, including Principal Component Analysis (PCA), Partial Least Squares Regression (PLSR), Random Forest (RF), and Support Vector Regression (SVR), was employed to discern predictive relationships between VIs and empirical yield data. Correlation analyses and model constructions were performed using various R packages, with model optimization facilitated by the 'caret' package. Data was partitioned into training and test sets with extensive cross-validation to ensure model validity. Model accuracy was evaluated using coefficient of determination ($R^2$) (Eq. 1), Root Mean Square Error (RMSE) (Eq. 2), Mean Absolute Error (MAE) (Eq. 3), and Residual Prediction Deviation (RPD) (Eq. 4), with higher $R^2$ and lower RMSE and MAE indicating improved model precision. An RPD above 2.5 signifies excellent predictive ability. The equations used for these metrics incorporate estimated and measured values, their averages, and standard deviations.

$$R^2 = \sum_{i=1}^{n}(x_i - \bar{x})^2\ (y_i - \bar{y})^2\ /\ \sum_{i=1}^{n}(x_i - \bar{x})^2\ \sum_{i-1}^{n}(y_i - \bar{y})^2 \quad \text{Eq. 1}$$

$$RMSE = \sqrt{1/_k\ \sum_{i=1}^{n}(x_i - y_i)^2} \quad \text{Eq. 2}$$

$$MAE = \sum_{i=1}^{n}|x_i - y_i|\ /\ k \quad \text{Eq. 3}$$

$$RPD = SD_{y_i}\ /\ RMSE \quad \text{Eq. 4}$$

# 3 Results and Conclusions

## 3.1 Yield Prediction models

#### 3.1.1 Principal component analysis and Partial Least Square Regression

The PCA models, constructed for BBCH40, BBCH65, and BBCH80 growth stages, displayed substantial efficacy in isolating key variations from a set of 35 vegetation indices, thereby mitigating multicollinearity. Notably, the BBCH65 PCA model, with an $R^2$ of 0.93 and an RMSE of 0.41 t/ha$^{-1}$ in the training set and an $R^2$ of 0.92 and RMSE of 0.42 t/ha$^{-1}$ in the test set, outperformed the other stages, indicating a significant alignment of principal components with GY at this mid-season stage (Fig. 1). Conversely, the PLSR models, while employing the same stage-based configuration, leveraged a broader component array, particularly at the BBCH80 stage with five components, culminating in an exceptional training set performance ($R^2$ = 0.97, RMSE = 0.28 t/ha$^{-1}$) and a robust test set outcome ($R^2$ = 0.94, RMSE = 0.41t/ha$^{-1}$) (Fig. 1). Such results underscore the PLSR model's superior predictive accuracy, especially as the crop approaches maturation. The nuanced selection of the PLSR components, corroborated by an "elbow point" analysis, highlights its strategic reduction of RMSE values, a vital consideration in predictive model optimization. This analysis, grounded in empirical data, advocates for the PLSR model's deployment in later growth stages of wheat, given its heightened correlation coefficients with AGB, a critical determinant of GY. In essence, while PCA offers valuable insights during the vegetative growth phase, PLSR's integration of complex spectral data presents a more robust framework for yield prediction.

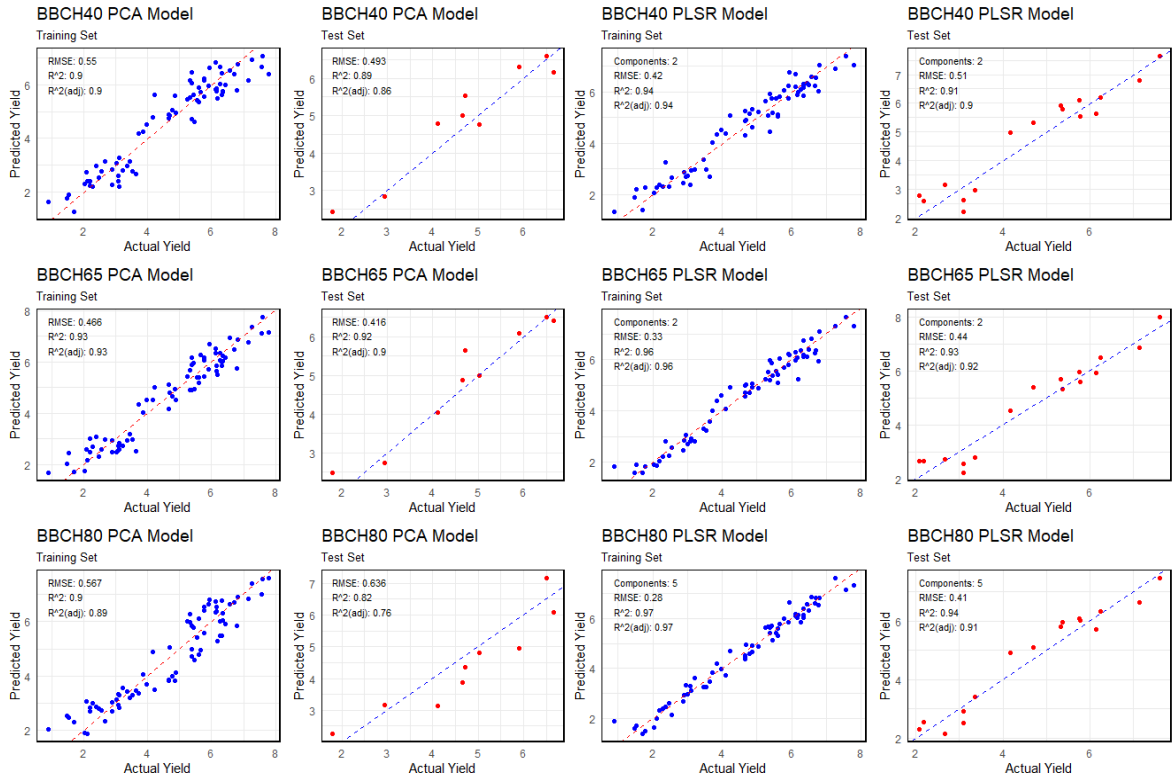


Fig. 1: Comparison of the prediction of GY using different PCA and PLSR models for the training and test datasets

### 3.1.2 Random Forest and Support Vector Regression

RF models showcased a variable performance across different configurations. Model 1, with an mtry value of 12 (Tab. 1), demonstrated a strong correlation in training ($R^2 = 0.9839$) but suffered a performance drop in testing ($R^2 = 0.8774$), as indicated by an increase in RMSE to 0.614 t/ha$^{-1}$. Model 2, however, with a higher mtry value of 31, sustained its predictive accuracy more consistently, evidenced by an $R^2$ of 0.9878 in training and a notable $R^2$ of 0.9049 in testing, alongside an RMSE of 0.195 t/ha$^{-1}$ and 0.536 t/ha$^{-1}$, respectively (Fig.2). Model 3 paralleled the performance pattern of Model 1 during testing phases, albeit with a slightly lower $R^2$ of 0.8844 and an RMSE of 0.585 t/ha$^{-1}$. These models' robustness was further characterized by the significance of various features, with CCCI, NDWI, and OSAVI_REDEDGE emerging as key predictors across models.

Conversely, the SVR models, predicated on Gaussian Radial Basis functions and sensitive to data scaling, required meticulous normalization. The sigma value and cost parameter (C) tuning were pivotal, as exemplified by the first SVR model's cross-validation RMSE of 0.533 t/ha$^{-1}$ and $R^2$ of 0.91, which slightly deteriorated in the test set to an RMSE of 0.664 t/ha$^{-1}$ and $R^2$ of 0.85. The subsequent models followed suit, with the third SVR model showcasing superior cross-validation results (RMSE = 0.412 t/ha$^{-1}$, $R^2 = 0.96$), indicating a robust model that was slightly less predictive in the test set (RMSE = 0.701 t/ ha$^{-1}$, $R^2 = 0.83$).

The SVR models generally exhibited higher precision during cross-validation compared to the RF models, as indicated by lower RMSE values and higher $R^2$. Particularly, the third SVR model's cross-validation performance was exemplary, possibly due to its optimized sigma parameter and cost setting. However, the RF models, especially Model 2, demonstrated

remarkable stability between training and testing phases, suggesting a better generalization capability. Overall, RF models potentially offer more robust generalization across datasets, whereas SVR models excel in model precision during the validation process.

Tab. 1: Descriptive statistic of RF models averaged trained performance across 10 folds using different mtry selection.

| BBCH | mtry | RMSE | $R^2$ | MAE | RPD |
|---|---|---|---|---|---|
| 40 | *12* | 0.515 | 0.91 | 0.42 | 2.87 |
| 65 | *31* | 0.461 | 0.94 | 0.38 | 3.29 |
| 80 | *8* | 0.461 | 0.94 | 0.4 | 3.01 |

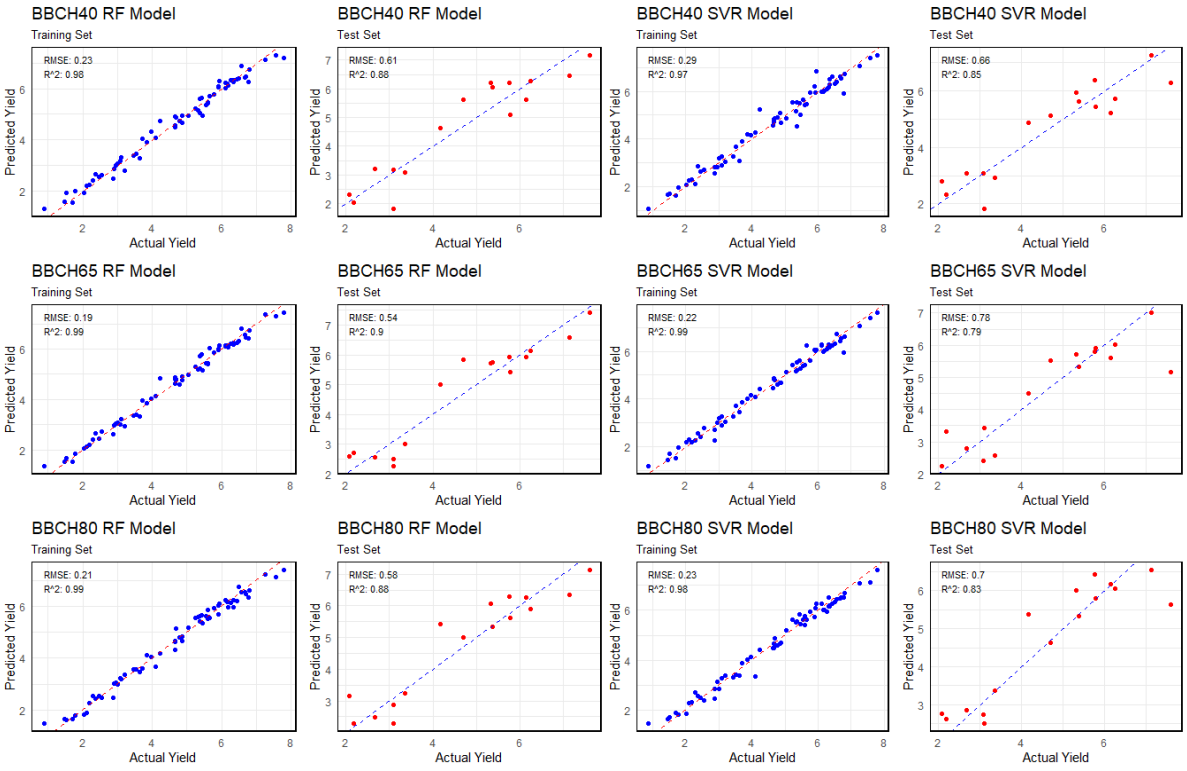


Fig. 2: Comparison of the prediction of GY using different RF and SVR models for the training and test datasets

## 3.2 Conclusions

In conclusion, the integrated analysis of PCA, PLSR, RF, and SVR models provides a comprehensive landscape of their capabilities and constraints in the context of wheat yield prediction. The PCA models, while adept at multicollinearity reduction, showcase optimal performance at the BBCH65 stage, but they are constrained by the diminishing marginal returns on variance explanation. On the other hand, the PLSR models demonstrate an enhanced capacity for predictive accuracy, particularly with a five-component model at the BBCH80 stage, suggesting a nuanced selection of components is key for model optimization. RF models emerge as robust and generalizable predictors, with the importance of features such as CCCI and NDWI highlighting the models' sensitivity to specific vegetation indices. SVR models, with their superior precision in cross-validation, underscore the importance of meticulous parameter tuning and normalization.

# 4 References


BAURIEGEL, E., GIEBEL, A. & HERPPICH, W., 2010: Rapid Fusarium head blight detection on winter wheat ears using chlorophyll fluorescence imaging. Journal of Applied Botany and Food Quality, **83**, 196-203.

BENDIG, J., BOLTEN, A., BENNERTZ, S., BROSCHEIT, J., EICHFUSS, S. & BARETH, G., 2014: Estimating Biomass of Barley Using Crop Surface Models (CSMs) Derived from UAV-Based RGB Imaging. Remote Sensing, **6**(11), 10395-10412, https://doi.org/10.3390/rs61110395.

DONOHUE, R. J., RODERICK, M. L., MCVICAR, T. R. & YANG, Y., 2017: A simple hypothesis of how leaf and canopy-level transpiration and assimilation respond to elevated CO2 reveals distinct response patterns between disturbed and undisturbed vegetation. Journal of Geophysical Research: Biogeosciences, **122**(1), 168-184, https://doi.org/10.1002/2016JG003505.

FARALLI, M., MATTHEWS, J. & LAWSON, T., 2019: Exploiting natural variation and genetic manipulation of stomatal conductance for crop improvement. Current Opinion in Plant Biology, **49**, 1-7, https://doi.org/10.1016/j.pbi.2019.01.003.

FURBANK, R. T., SHARWOOD, R., ESTAVILLO, G. M., SILVA-PEREZ, V. & CONDON, A. G., 2020: Photons to food: genetic improvement of cereal crop photosynthesis. Journal of Experimental Botany, **71**(7), 2226-2238, https://doi.org/10.1093/jxb/eraa077.

GUIDI, L. & CALATAYUD, A., 2014: Non-invasive tools to estimate stress-induced changes in photosynthetic performance in plants inhabiting Mediterranean areas. Environ. and Experimental Botany, **103**, 42-52, https://doi.org/10.1016/j.envexpbot.2013.12.007.

GUIDI, L., LO PICCOLO, E. & LANDI, M., 2019: Chlorophyll Fluorescence, Photoinhibition and Abiotic Stress: Does it Make Any Difference the Fact to Be a C3 or C4 Species? Frontiers in Plant Science, **10**, https://doi.org/10.3389/fpls.2019.00174.

HERZIG, P., BORRMANN, P., KNAUER, U., KLÜCK, H.-C., KILIAS, D., SEIFFERT, U., PILLEN, K. & MAURER, A., 2021: Evaluation of RGB and Multispectral Unmanned Aerial Vehicle (UAV) Imagery for High-Throughput Phenotyping and Yield Prediction in Barley Breeding. Remote Sensing, **13**(14), 2670, https://doi.org/10.3390/rs13142670.

LAWSON, T., VON CAEMMERER, S. & BAROLI, I., 2011: Photosynthesis and Stomatal Behaviour. Progress in Botany, **72**, 265-304.

LIU, S., BARET, F., ALLARD, D., JIN, X., ANDRIEU, B., BURGER, P., HEMMERLÉ, M. & COMAR, A., 2017: A method to estimate plant density and plant spacing heterogeneity: application to wheat crops. Plant Methods, **13**(1), 38, https://doi.org/10.1186/s13007-017-0187-1.

LIU, W., LI, Y., LIU, J. & JIANG, J., 2021: Estimation of Plant Height and Aboveground Biomass of Toona sinensis under Drought Stress Using RGB-D Imaging. Forests, **12**(12), 1747, https://doi.org/10.3390/f12121747.

MAKANZA, R., ZAMAN-ALLAH, M., CAIRNS, J. E., MAGOROKOSHO, C., TAREKEGNE, A., OLSEN, M. & PRASANNA, B. M., 2018: High-Throughput Phenotyping of Canopy Cover and Senescence in Maize Field Trials Using Aerial Digital Canopy Imaging. Remote Sensing, **10**(2), 330, https://doi.org/10.3390/rs10020330.

PARRY, M. A. J., REYNOLDS, M., SALVUCCI, M. E., RAINES, C., ANDRALOJC, P. J., ZHU, X.-G., PRICE, G. D., CONDON, A. G. & FURBANK, R. T., 2010: Raising yield potential of wheat. II. Increasing photosynthetic capacity and efficiency. Journal of Experimental Botany, **62**(2), 453-467, https://doi.org/10.1093/jxb/erq304.

PAUDEL, D., BOOGAARD, H., DE WIT, A., VAN DER VELDE, M., CLAVERIE, M., NISINI, L., JANSSEN, S., OSINGA, S. & ATHANASIADIS, I. N., 2022: Machine learning for regional crop yield forecasting in Europe. Field Crops Research, **276**, 108377, https://doi.org/10.1016/j.fcr.2021.108377.

PENNISI, G., BLASIOLI, S., CELLINI, A., MAIA, L., CREPALDI, A., BRASCHI, I., SPINELLI, F., NICOLA, S., FERNANDEZ, J. A., STANGHELLINI, C., MARCELIS, L. F. M., ORSINI, F., & GIANQUINTO, G., 2019: Unraveling the Role of Red:Blue LED Lights on Resource Use Efficiency and Nutritional Properties of Indoor Grown Sweet Basil. Frontiers in Plant Science, **10**, https://doi.org/10.3389/fpls.2019.00305.

PREY, L. & SCHMIDHALTER, U., 2019: Simulation of satellite reflectance data using high-frequency ground based hyperspectral canopy measurements for in-season estimation of grain yield and grain nitrogen status in winter wheat. ISPRS J. Photogramm. Remote Sens., **149**, 176-187, https://doi.org/10.1016/j.isprsjprs.2019.01.023.

RAINES, C. A., 2010: Increasing Photosynthetic Carbon Assimilation in C3 Plants to Improve Crop Yield: Current and Future Strategies. Plant Physiology, **155**(1), 36-42, https://doi.org/10.1104/pp.110.168559.

ROCHE, D., 2015: Stomatal Conductance Is Essential for Higher Yield Potential of C3 Crops. Critical Reviews in Plant Sciences, **34**(4), 429-453.

SÁNCHEZ-MOREIRAS, A. M., GRAÑA, E., REIGOSA, M. J. & ARANITI, F., 2020: Imaging of Chlorophyll a Fluorescence in Natural Compound-Induced Stress Detection. Frontiers in Plant Science, **11**, https://doi.org/10.3389/fpls.2020.583590.

TANAKA, Y., SUGANO, S. S., SHIMADA, T. & HARA-NISHIMURA, I., 2013: Enhancement of leaf photosynthetic capacity through increased stomatal density in Arabidopsis. New Phytologist, **198**(3), 757-764, https://doi.org/10.1111/nph.12186.

TARVAINEN, L., RÄNTFORS, M. & WALLIN, G., 2015: Seasonal and within-canopy variation in shoot-scale resource-use efficiency trade-offs in a Norway spruce stand. Plant, Cell & Environment, **38**(11), 2487-2496, https://doi.org/10.1111/pce.12565.

TAUSZ-POSCH, S., ARMSTRONG, R. & TAUSZ, M., 2014: Nutrient Use and Nutrient Use Efficiency of Crops in a High CO2 Atmosphere. Nutrient Use Efficiency in Plants: Concepts and Approaches, 229-252, https://doi.org/10.1007/978-3-319-10635-9_9.

WALTER, J., EDWARDS, J., MCDONALD, G. & KUCHEL, H., 2018: Photogrammetry for the estimation of wheat biomass and harvest index. Field Crops Research, **216**, 165-174. https://doi.org/10.1016/j.fcr.2017.11.024.

YAMORI, W. & SHIKANAI, T., 2016: Physiological Functions of Cyclic Electron Transport Around Photosystem I in Sustaining Photosynthesis and Plant Growth. Ann. Review of Plant Biology, **67**(1), 81-106. https://doi.org/10.1146/annurev-arplant-043015-112002.

YAO, J., SUN, D., CEN, H., XU, H., WENG, H., YUAN, F. & HE, Y., 2018: Phenotyping of Arabidopsis Drought Stress Response Using Kinetic Chlorophyll Fluorescence and Multicolor Fluorescence Imaging. Frontiers in Plant Science, **9**, https://doi.org/10.3389/fpls.2018.00603.

YUE, J., YANG, G., TIAN, Q., FENG, H., XU, K. & ZHOU, C., 2019: Estimate of winter-wheat above-ground biomass based on UAV ultrahigh-ground-resolution image textures and vegetation indices. ISPRS J. Photogramm. Remote Sens., **150**, 226-244, https://doi.org/10.1016/j.isprsjprs.2019.02.022.

ZHANG, S. Y., ZHANG, G. C., LIU, X. & XIA, J. B., 2013: The responses of photosynthetic rate and stomatal conductance of Fraxinus rhynchophylla to differences in CO<sub>2</sub> concentration and soil moisture. Photosynthetica, **51**(3), 359-369.